Microchimica Acta (2021) 188: 28
https://doi.org/10.1007/s00604-020-04659-z

ORIGINAL PAPER

A photoelectrochemical enzyme biosensor based on functionalized hematite microcubes for rutin determination by square-wave voltammetry

Gabriel J. Mattos[1] · Carlos A. R. Salamanca-Neto[1] · Eduardo C. M. Barbosa[1] · Pedro H. C. Camargo[2] · Robert F. H. Dekker[3] · Aneli M. Barbosa-Dekker · Elen R. Sartori[1]

Received: 24 June 2020 / Accepted: 19 November 2020 / Published online: 6 January 2021

Abstract

A photoelectrochemical biosensing strategy for the highly sensitive detection of the flavonoid rutin was developed by synergizing the photoelectrocatalytic properties of hematite (α-Fe_2O_3) decorated with palladium nanoparticles (PdNPs) and the biocatalysis towards laccase-based reactions. The integration of α-Fe_2O_3.PdNPs with a polyphenol oxidase as a biorecognition element yields a novel biosensing platform. Under visible light irradiation, the photoactive biocomposite can generate a stable photocurrent, which was found to be directly dependent upon the concentration of rutin. Under the optimal experimental conditions, the cathodic photocurrent, measured at 0.33 V vs. Ag/AgCl, from the square-wave voltammograms presented a linear dependence on the rutin concentration within the range of $0.008–30.0 \times 10^{-8}$ mol L^{-1} (sensitivity: 1.7 μA·($\times 10^{-8}$ M^{-1})·cm^{-2}), with an experimental detection limit ($S/N = 3$) of 8.4×10^{-11} mol L^{-1}. The proposed biosensor device presented good selectivity towards rutin in the presence of various organic compounds and inorganic ions, demonstrating the potential application of this biosensing platform in complex matrices. This bioanalytical device also exhibited excellent operational and analytical properties, such as intra-day (standard deviation, SD = 0.21%) and inter-day (SD = 1.30%) repeatability, and long storage stability (SD = 2.80% over 30 days).

Keywords Biosensor · Iron oxide · Laccase · Photoelectrocatalysis · Voltammetry · Nanomaterials · Flavonoids · Rutin

Introduction

Photoelectrochemical (PEC) processes are a promising approach in quantitative analysis to transform chemical energy into analytical signals under light incidence and a specific applied potential [1]. PEC biosensing technology has attracted extensive attention because of its property in detecting several molecules through the photocurrent generated from reduction/oxidation on a chemically selective surface.

Photocatalytic nanostructured materials have been coupled to carbon-based electrodes, as both display high electrocatalytic activity, and biocompatibility to obtain direct contact with biomaterials (e.g., enzymes) acting as biorecognition elements to enhance the selectivity of PEC analysis [2, 3]. Nanostructured semiconductors have been explored for PEC applications because of their unique photophysical properties. These nanometric materials provide an efficient signal-transducing mode, producing photoexcited carriers e^- and h^+ in their conductive (CB) and valence bands (VB), respectively [4, 5]. Titanium dioxide (TiO_2) is one of the most used semiconductors owing to its remarkable characteristics, such as biocompatibility, photochemical stability, and facile surface modification, providing several (bio)sensing applications [6–8]. However, the use of unmodified TiO_2 for PEC bioanalysis has some limitations mainly because it is a wide bandgap semiconducting material, requiring UV wavelength irradiation for its excitation. The effect of UV irradiation can

✉ Elen R. Sartori
elensartori@uel.br

[1] Departamento de Química, Laboratório de Eletroanalítica e Sensores, Universidade Estadual de Londrina, Centro de Ciências Exatas, Rodovia Celso Garcia Cid, PR 445, Km 380, Cx.P. 10.011, Londrina, PR CEP: 86057-970, Brazil

[2] Departamento de Química Fundamental, Universidade de São Paulo, Instituto de Química, São Paulo, SP CEP: 05508-000, Brazil

[3] Programa de Pós-Graduação em Engenharia Ambiental, Universidade Tecnológica Federal do Paraná, Câmpus Londrina, Londrina, PR CEP: 86036-370, Brazil

cause irreversible damage to ligand-protein structures such as enzymes, causing their denaturation [9].

Iron oxide-based materials have been widely explored for photocatalytic purposes due to their low bandgap [10]. Hematite (α-Fe_2O_3) is the most stable iron oxide at ambient condition, and an environmentally friendly n-type semiconductor [11]. Some of its application areas include drug delivery [12], pigments [13], photocatalysis [14], solar cells [15], and (bio)sensors [16, 17]. Also, many attempts have been made to modify semiconductors by decoration with noble metal nanoparticles (Ag, Au, Pt, and Pd), which act as electron acceptors (avoiding recombination processes) [18, 19], and immobilization sites for biomolecules in the development of photoelectrochemical biodevices. The use of PEC enzyme biosensors has attracted remarkable research interest as a result of their versatility, good stability, and the selectivity/specificity of the enzyme-catalyzed reactions under mild conditions [20]. However, the procedure of immobilizing enzymes onto noble metal nanoparticles decorating iron oxide (hematite) microcubes has not yet been considered for assembling a photoactive biocomposite and is the main objective of our paper.

The interest in using laccase (LCE; EC 1.10.3.2) as a biorecognition element for monitoring (poly)phenolic compounds electrochemically has increased recently, considering their specific and peculiar properties. The ability of laccases to catalyze electron transfer reactions without cofactors, oxidize (poly)phenolic compounds, and possess great stability, has resulted in a wide spectrum of applications in several commercial sectors, such as in the pulp/paper industry [21] and biosensing technology [22, 23]. The ligninolytic ascomyceteous fungus *Botryosphaeria rhodina* isolate MAMB-05 produces an extracellular LCE constitutively, and the induction by veratryl alcohol results in higher enzyme titers over the constitutive levels of the enzyme produced [24].

The monitoring of (poly)phenolics in the food industry, and for biomedical analysis, has become an area of growing interest over the development of portable, selective, and cost-effective analytical devices. Rutin (RTN) is a flavonoid (a sub-class of polyphenolics) widely distributed in nature (fruits/vegetables), and their antioxidant properties may be involved in assisting to prevent cancer, stroke, and cardiovascular-related diseases [25]. Intending to evaluate the possible impact of consuming foodstuffs and/or dietary supplements with high flavonoid levels, an appropriate method of food and biological fluids characterization based on quantitative analysis is necessary. Although spectrophotometric [26, 27] and chromatographic [28, 29] methods have been used for the determination of rutin, recent research in monitoring methods has focused on bioanalytical devices [30, 31]. Notwithstanding that the enzymatic PEC biosensor offers considerable advantages in terms of sensitivity, selectivity, and reduced time of assay, it has not yet been explored for the monitoring of RTN in real samples.

Taking the above features into account, the study reported herein describes for the first time the construction of a laccase-biosensor based on the immobilization of the enzyme onto palladium nanoparticles (PdNPs) decorating α-Fe_2O_3-faceted microcubes and employing a glassy carbon electrode (GCE) as the supporting electrochemical transducer. The electrochemical probe $[Fe(CN)_6]^{3-/4-}$ was employed to characterize this biosensing platform, denoted as GCE/(α-Fe_2O_3.PdNPs)-LCE, by electrochemical impedance spectroscopy (EIS). The analytical parameters of this novel fabricated PEC biosensor are described and compared with other (bio)sensors previously reported in the literature. After establishing the best operating conditions, the developed method using this PEC bioanalytical device was applied to quantify rutin in beverages and biological samples by square-wave voltammetry (SWV).

Experimental

Chemicals and instruments

The synthesis of hematite-faceted crystals decorated with PdNPs required the following chemicals: $Fe(NO_3)_3{\cdot}9H_2O$ ($\geq$ 99.0%), $Zn(CH_3COO)_2{\cdot}2H_2O$ ($\geq$ 98%), K_2PdCl_4 ($\geq$ 98.0%), PVP (polyvinylpyrrolidone, MW 55,000 g mol^{-1}), and hydroquinone ($\geq$ 99%). They, and rutin ($\geq$ 94.0%) and H_2SO_4 ($\geq$ 95.0%), were all obtained from Sigma-Aldrich (www.sigmaaldrich.com). Uric acid ($\geq$ 99.0%), NH_4OH ($\geq$ 30.0% NH_3), and $K_4[Fe(CN)_6]$ ($\geq$ 99.95%) were obtained from Synth (www.lojasynth.com/synth). All reagents were of analytical grade and used as received. Commercial beverage samples were acquired from a local supermarket in the city of Londrina.

All reagent solutions were prepared using ultra-purified water supplied by a Milli-Q system (Millipore®) with resistivity > 18 MΩ cm. Phosphate buffer (PB; 0.1 mol L^{-1}) was prepared using potassium monobasic phosphate and dibasic potassium phosphate (pH range from 4.0 to 8.0); these solutions were used as the supporting electrolyte throughout the electroanalytical experiments. For the electrochemical impedance spectroscopy (EIS) experiments, a KCl solution (0.1 mol L^{-1}, pH 7.5) was used. A RTN standard stock solution of 10 mmol L^{-1} was freshly prepared daily in 0.1 mol L^{-1} phosphate buffer at pH 6.0. Standard working solutions of RTN were prepared from the stock solutions by appropriate dilution.

For the characterization of the α-Fe_2O_3.PdNPs, a scanning electron microscope (JEOL FEG-SEM JSM 6330F; JEOL, Tokyo, Japan) operated at 5 kV was used to obtain images by scanning electron microscopy (SEM). Aqueous

suspensions of the samples were drop-cast on top of a silicon wafer and allowed to dry at room temperature.

An X-ray diffractometer (Bruker D2 Phaser; Bruker, Hamburg, Germany) was employed to acquire X-ray diffraction (XRD) patterns of the samples. A standard Cu Kα source was employed (l ¼ 1.54060 Å, 30 kV, 15 mA). The integration time was set to 0.75 s and step to 0.03°, with 2θ ranging from 20 to 80°. XRD samples were prepared by placing the samples on an acrylate sample holder.

Palladium (Pd) content was determined by flame atomic absorption spectrophotometry (FAAS; Shimadzu AA-6300; Shimadzu, Kyoto, Japan). Samples were digested using freshly prepared aqua regia.

Square-wave voltammetry and EIS measurements using the fabricated PEC biosensor were performed on a FRA2 μAutoLab Type III potentiostat/galvanostat (Metrohm Autolab B.V., The Netherlands), controlled with NOVA 2.1 software (www.metrohm-autolab.com/Products/Echem/Software). SW voltammograms were baseline-corrected by the average filter (peak width: 0.001). EIS experiments were performed in the range of 10 mHz to 100 kHz, and with a 10-mV (r.m.s.) ac perturbation for a 1 mmol L^{-1} $K_4[Fe(CN)_6]$ in 0.1 mol L^{-1} KCl solution.

A homemade photoreactor (black box) was used for the photoelectrochemical experiments; white light from a phosphor-converted light-emitting diode (LED, 450–475 nm) was focused on the electrode surface for the photoexcitation process.

A conventional three-electrode single-compartment glass cell was used at room temperature (25.0 ± 0.5 °C) for all experiments and comprised the PEC biosensor as the working electrode, Ag/AgCl (3.0 mol L^{-1} KCl) as the reference electrode, and a platinum plate as the auxiliary electrode. A stirring time of 30 s was used to ensure RTN was totally solubilized in the electrochemical cell.

All pH measurements were made at 25.0 ± 1.0 °C using a combined glass electrode with an Ag/AgCl (3.0 mol L^{-1} KCl) external reference electrode connected to a pH meter (model W3B; BEL, Sao Paulo, Brazil).

High-performance liquid chromatography (HPLC) for the determination of RTN was carried out using a LC Shimadzu chromatograph (Shimadzu, Sao Paulo, Brazil) coupled to a system with a LC-20AT pump, SIL-20 AC automatic injector, and SPD-M20A PDA detector, and an ACE 5 C-18 column (250 mm × 4.6 mm i.d., particle size: 5 μm) at 25.0 ± 1.0 °C. The mobile phase was methanol, acetic acid, and water (28:5:67). UV absorbance was monitored from 220 to 440 nm.

Synthesis of Pd nanoparticles onto α-Fe_2O_3-faceted crystals

In a typical procedure, 5.7 g of $Fe(NO_3)_3 \cdot 9H_2O$ was added to 70 mL of deionized water and stirred until all of the salt had dissolved. To this mixture 768 mg of $Zn(CH_3COO)_2 \cdot 2H_2O$ was added and stirred for 10 min at room temperature, followed thereafter by the addition of 70 mL of concentrated NH_4OH solution, which resulted in the formation of a brown precipitate. The mixture was then stirred for 15 min at room temperature and transferred into a capped Teflon-lined stainless-steel autoclave (220 mL capacity), heated to 160 °C for 16 h, and then allowed to cool to room temperature. The solution was then centrifuged (3158×*g* for 5 min), the precipitate recovered and well washed with water (5 times) followed by centrifugation in between the washing steps, and finally, washed with ethanol (2 times) followed by re-centrifuging to recover the precipitate. After the last wash, the precipitate recovered was dried under vacuum, producing about 2.0 g d.w (dry weight). of Fe_2O_3 microcubes.

To decorate the pre-formed microcubes, a suspension of Fe_2O_3 microcubes was prepared by adding 200 mg of the powder prepared as aforementioned to 10 mL of water, and the mixture sonicated in an ultrasound bath for 10 min. To this was added 30 mL of an aqueous solution of hydroquinone (10 mmol L^{-1}), followed by the addition of 50 mL of an aqueous solution of PVP (7 g L^{-1}), and the mixture heated at 90 °C for 10 min whilst stirring. Lastly, 30 mL of K_2PdCl_4 (4 mmol L^{-1}) was added to the mixture and left for 1 h at 90 °C under vigorous stirring to produce the Pd/Fe_2O_3 material. The latter was recovered by centrifugation, and then washed with ethanol (5 times, 3158×*g*, 5 min), and the recovered material left to dry overnight in a vacuum oven at 70 °C. To treat Pd/Fe_2O_3, the samples were placed in a furnace and heated at 400 °C for 1 h with an airflow of 10 mL min^{-1}, and then allowed to cool to room temperature.

Immobilizing laccase onto the photoactive α-Fe_2O_3.PdNPs support: PEC biosensor architecture

A bare glassy carbon electrode (GCE; Tokai Carbon Co. Ltd., Japan, 3-mm diameter) was used as the supporting transducer. Prior to its use, the GCE was carefully polished with a 0.3-μm alumina slurry on a polishing cloth followed by ultrasonically cleaning with ultrapure water for 3 min and then allowed to dry at room temperature. For the construction of the biosensor, laccase was obtained from *B. rhodina* MAMB-05 as previously described and was assayed against ABTS (2,2′-Azinobis(3-ethylbenzothiazoline-6-sulfonic acid)) [32]. The immobilization of the biorecognition element was performed by incubating laccase (13.8 U mL^{-1}) in 500 μL of PB (pH 6.0) containing α-Fe_2O_3.PdNPs (1 mg mL^{-1}, 1.94% Pd) for 2 h at 37 °C. Following the physical adsorption step of LCE onto the photoactive material, an aliquot of the final solution (5 μL) was layered onto the surface of the polished GCE, and the electrode cured for 2 h at room temperature. The developed PEC biosensor was stored at 4 °C (refrigerator) when not in use.

For comparative purposes, the following sensors were also prepared: unmodified GCE, GCE/PdNPs, and GCE surface-layered with α-Fe_2O_3.PdNPs.

Measurement procedures

SW voltammograms (SWV) were obtained for the different sensors (GCE, GCE/PdNPs, GCE/α-Fe_2O_3.PdNPs, and GCE/α-Fe_2O_3.PdNPs-LCE) in the presence of RTN to evaluate the electrochemical contribution of each modifying procedure of the working electrode fabricated. The voltammetric measurements were performed using an electrochemical cell containing 10 mL of PB (pH 6.0) and a scanning potential range from 0.5 to − 0.5 V. Measurements were carried out in triplicate to ensure significance of the results.

The analytical curve for RTN was constructed by adding aliquots of the RTN standard working solution (1.0×10^{-5} mol L^{-1}) into the electrochemical cell containing 10 mL of PB (pH 6.0), and SWV measurements performed in triplicate. The instrumental parameters of the SWV technique optimized for the determination of RTN were: frequency (f) = 50 Hz, amplitude (a) = 50 mV, scan increment (ΔE_S) = 3 mV). The limit of detection (LOD) was experimentally determined at S/N = 3. These procedures were performed and compared under the *light-off* (black box) and *light-on* (white light from LED) modes.

Preparation of diverse samples for the determination of rutin

The beverage samples were red wine and green tea and were directly analyzed without any previous treatment. For this purpose, 200 μL of each sample was added into the electrochemical cell, and standard addition analysis was accomplished by measuring the current intensity at 0.33 V vs. Ag/AgCl, before and after the addition of aliquots of the RTN standard working solution (1.0×10^{-5} mol L^{-1}). HPLC determination of RTN was carried out on the green tea and red wine samples by the method as described by Tarola et al. [33], in order to check the accuracy of the proposed method employing the PEC biosensor.

Human urine was used as an example of biological sample to evaluate whether concomitant substances interfered during the electroanalysis of RTN. A urine sample was obtained from a healthy male adult volunteer (male, 22-year-old, non-smoker) immediately prior to the experimental measurements. For the electrochemical analysis, 0.1 mL of fresh urine was added to the electrochemical cell containing 10 mL of PB (pH 6.0). The solution was then spiked with the standard working solution of RTN (1.0×10^{-5} mol L^{-1}) to achieve a concentration of 1.0 and 3.0 mg L^{-1}. Addition and recovery tests were performed on the urine sample to verify the accuracy of the method in the analysis of biological fluids.

Results and discussion

Physical-chemical characterization of the α-Fe_2O_3.PdNPs microcubes

The synthesized α-Fe_2O_3.PdNPs were characterized regarding their morphological, structural, and photoactive properties employing scanning electron microscopy (SEM), X-ray diffraction (XRD), Raman spectroscopy, and diffuse reflectance spectroscopy. Discussion of these aspects is presented in Electronic Supplementary Material (ESM).

Photoelectrochemical characterization of the proposed PEC biosensor by electrochemical impedance spectroscopy

PEC processes can be studied by methods based on the monitoring of electron transfer kinetics under light excitation. In the work reported herein, the photoelectrochemical characterization of the following fabricated electrochemical sensor devices: GCE, GCE/α-Fe_2O_3.PdNPs, and GCE/(α-Fe_2O_3.PdNPs)-LCE was performed by impedance measurements using the classical electroactive probe, hexacyanoferrate $[Fe(CN)_6]^{4-/3-}$. The Nyquist plot of an electrochemical impedance spectrum usually consists of a semi-circular region at the higher frequencies, wherein the diameter represents the charge transfer resistance, and the straight line at an angle of 45° to the real axis at lower frequencies, represents the diffusion process (mass transfer control). The Randles equivalent circuit includes only solution resistance (R_S), a parallel combination of a double-layer capacitor (C_{pe}—constant phase element), a charge transfer or polarization resistance (R_{CT}), and a specific element of diffusion (Warburg element, W), as represented in the circuit shown in Fig. 1 (*inset*).

EIS is often employed to monitor interfacial properties during the construction of a modified electrode. As seen in Fig. 1, the introduction of α-Fe_2O_3.PdNPs onto GCE (GCE/α-Fe_2O_3.PdNPs) resulted in a decrease in the semi-circle diameter (R_{CT} 0.58 kΩ) compared with the bare GCE (R_{CT} 1.1 kΩ), suggesting that the nanomaterial, as expected, increased the electron transfer rate in the electrochemical system. When the biocomposite (α-Fe_2O_3.PdNPs)-LCE) was deposited onto the GCE surface (CGE/(α-Fe_2O_3.PdNPs)-LCE), the resistance of the device reached its highest value (R_{CT} 1.5 kΩ) indicating the formation of a biocatalytic film on the electrode to decrease the accessibility of the electrochemical probe. The impedance experiment was performed at pH 7.5, which according to [34], is above the isoelectric point of laccases, in general. Under this condition, the enzyme is negatively charged causing an electric repulsion with the $[Fe(CN)_6]^{4-/3-}$ probe and resulting in the high measured resistance. These results further confirm the effective immobilization of LCE onto the nanostructured material for the

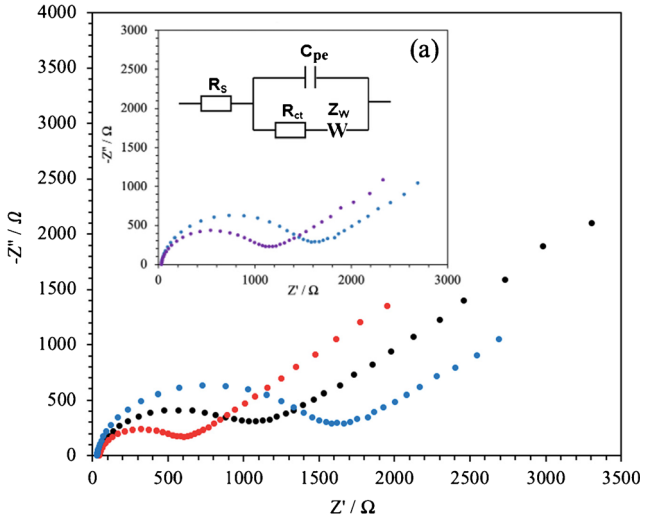

Fig. 1 Electrochemical impedance spectra for (●) GCE, (●) GCE/α-Fe_2O_3.PdNPs, and (●) GCE/(α-Fe_2O_3.PdNPs)-LCE (the developed PEC biosensor*)* in 0.1 mol L^{-1} KCl solution containing 1.0 mmol L^{-1} $[Fe(CN)_6]^{4-/3-}$ at pH 7.5, open circuit mode (*inset* in (**a**) circuit model; R_{SOL}—solution resistance, R_{CT}—charge transfer resistance, and CPE—constant phase element), 10 mV amplitude and frequency range of 10 mHz to 100 kHz. *Inset:* (**a**) electrochemical impedance spectra for the developed PEC biosensor (●) *light-off* mode and (●) *light-on* mode in 0.1 mol L^{-1} KCl solution containing 1.0 mmol L^{-1} $[Fe(CN)_6]^{4-/3-}$ at pH 7.5

construction of the photoelectrochemical bioanalytical device. Previous works in the literature reported on metallic palladium complexes based on the Pd-N interaction, containing ligand sets that are biologically relevant, including species as amino acids, peptides, and other inorganics [35]. This method of immobilization presents high operational stability and low-cost fabrication and allows enzyme stability to pH and temperature.

In order to attest the photocatalytic effects of the α-Fe_2O_3.PdNPs microcubes, Fig. 1 (*inset* a) presents the Nyquist plot of the EI spectrum for the proposed PEC biosensor under visible light excitation. As shown, there was a remarkable decrease in the electron transfer resistance (R_{CT} 1.15 kΩ) compared to the *light-off* mode (R_{CT} 1.5 kΩ). Under irradiation of visible light, the overall mechanism of the PEC process involves (i) light absorption by the α-Fe_2O_3.PdNPs microcubes, (ii) photoexcited carrier generation of electrons (e^-) and holes (h^+), and (iii) photoexcited electrons are ejected from the conduction band (CB) towards the PdNPs, which act as an intermediate charge acceptor. Finally, the electron is transferred to the electrode surface. Meantime, the photoexcited holes in the valence band (VB) of the α-Fe_2O_3.PdNPs microcubes are scavenged by the electroactive probe present in the electrolyte. The photoelectrocatalytic process as described can be used to effectively decrease the electron transfer resistance.

Electrochemical behavior of rutin on the GCE/(α-Fe_2O_3.PdNPs)-LCE biosensor

According to the mechanism of laccase-catalyzed reactions [21], rutin (a polyphenolic compound) in its reduced form is oxidized by laccase to *o*-quinone (Fig. 2a). The *o*-quinone generated is then electrochemically reduced on the surface of the photoelectrochemical device at 0.33 V vs. Ag/AgCl to rutin; as shown schematically in Fig. 2b. Under visible light irradiation, the electrons from the conduction band are transferred to PdNPs (the primary charge acceptor), and then, in turn, are passed on to the final electron acceptor, *o*-quinone generated by the biocatalytic oxidation of RTN. During this catalytic process, the photoholes in the valence band of the hematite particles are scavenged by the charge from the electrode surface.

Figure 2c displays the square-wave voltammograms obtained using the different fabricated sensors (GCE, GCE/PdNPs, GCE/α-Fe_2O_3.PdNPs, and GCE/(α-Fe_2O_3.PdNPs)-LCE) to evaluate the contribution of each modifier on signal amplification for the electrochemical reduction of *o*-quinone. Based upon the presented behavior, the electron transfer at the electrode/solution interface is favored by the electrocatalysis of the PdNPs (Fig. 2c, signal B), compared with the unmodified GCE (Fig. 2c, signal A). When this nanomaterial is deposited on the α-Fe_2O_3 microcubes surface, its electrocatalytic properties are maintained, as shown in Fig. 2c, signal C. Laccase's activity confers selectivity on the proposed device and results in high concentrations of the oxidized species (*o*-quinone) in solution, which results in a greater signal of current density arising from the electrochemical reduction. As can be seen in Fig. 2c, signal E, the highest cathodic peak current was obtained employing GCE/(α-Fe_2O_3.PdNPs)-LCE (*light-on*), due to the photoactive properties of α-Fe_2O_3. The PEC process combined with the biocatalytic oxidation of RTN resulted in the best performance for the proposed method, and consequently, the GCE/(α-Fe_2O_3.PdNPs)-LCE (*light-on* mode) device was chosen as the working electrode for the continuing experiments.

The stability and maintenance of the GCE/(α-Fe_2O_3.PdNPs)-LCE biosensor was assessed with regard to long-term storage. For this purpose, the electrochemical response was monitored using a standard solution of RTN (1.5×10^{-7} mol L^{-1}) for repetitive measurements over several days. After each electrochemical measurement, the PEC biosensor was rinsed and stored at 4.0 °C (refrigerator). After 30 days (longest period tested) of these sequential measurements, we observed that the cathodic current signals showed a standard deviation (SD) of 2.8% (*light-on*) (data presented in the ESM – Fig. ESM5). We conclude that the stability of enzyme activity on the sensor was attributed to the preservation of the three-dimensional structure of the protein chain due to the efficient immobilization onto the nanostructured photoactive support.

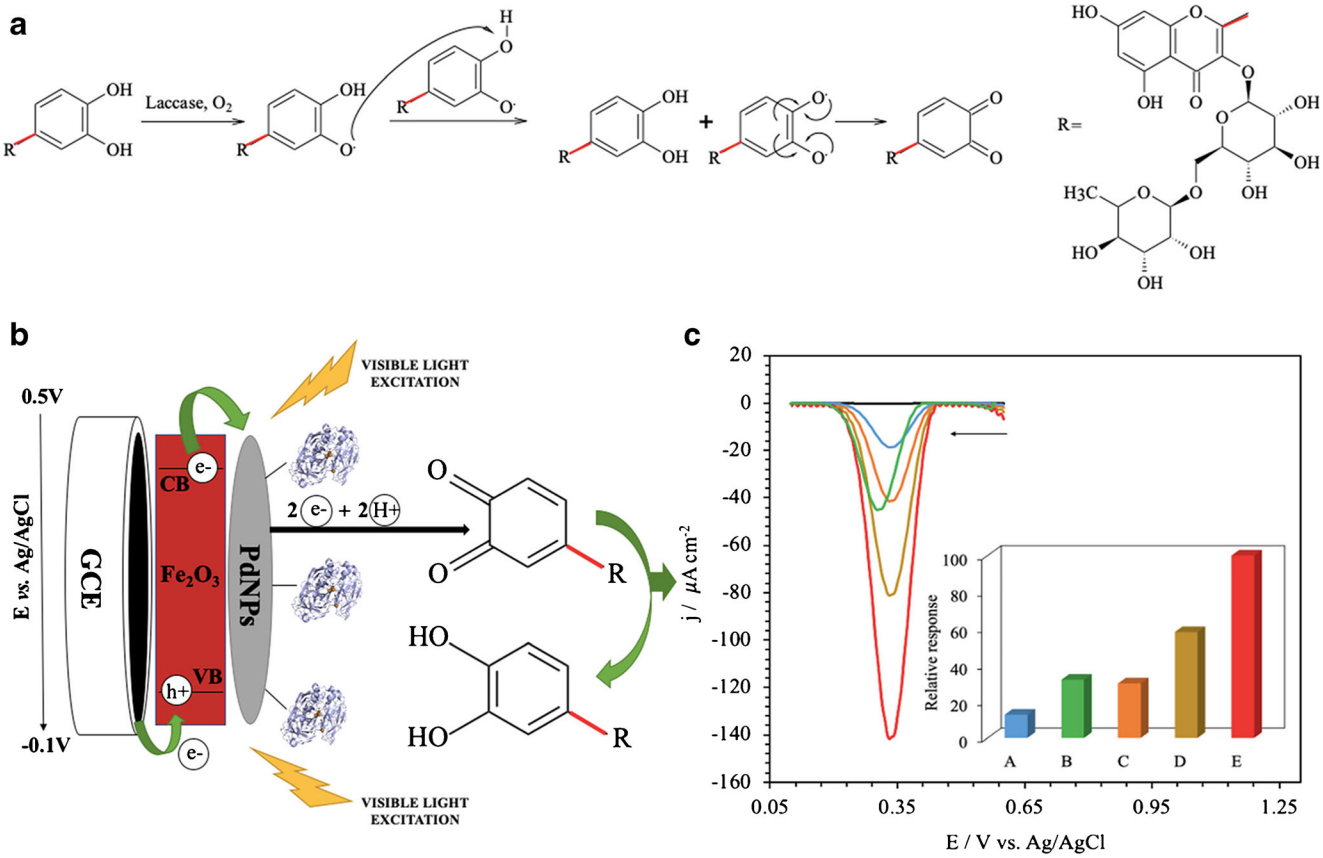

Fig. 2 (**a**) Laccase-initiated disproportionation of rutin into *o*-quinone, (**b**) Schematic diagram of electron transfer–based photoelectrochemical detection of rutin, and (**c**) SW voltammograms obtained using the electrodes (A) GCE, (B) GCE/PdNPs, (C) GCE/α-Fe_2O_3.PdNPs, (D) GCE/(α-Fe_2O_3.PdNPs)-LCE (*light-off* mode), and (E) GCE/(α-Fe_2O_3.PdNPs)-LCE (*light-on* mode) in PB (pH 6.0) containing 45.0 μmol L^{-1} rutin. SWV parameters: $f = 30$ Hz, $a = 50$ mV, and $\Delta E_S = 2$ mV. *Inset*: relative responses for the different sensors evaluated

Selection of analytical parameters for monitoring polyphenol and determination of the apparent Michaelis-Menten constant

Parameters related to the biosensor composition were investigated in order to guarantee the best analytical performance. The effect of the amount of LCE for immobilization onto the α-Fe_2O_3.PdNPs microcubes was investigated using enzyme activities of 5.3, 13.8, and 20.7 U mL^{-1}. The highest cathodic peak current was found for an activity loading of 13.8 U mL^{-1} of LCE during the adsorption procedure. Based upon these results, a LCE activity of 13.8 U mL^{-1} was used as optimal enzyme loading for the construction of further biosensor devices.

The pH of the supporting electrolyte affects the ionizable groups on the enzyme structure. Furthermore, pH variation was found to strongly influence LCE activity and, consequently, the photoelectrochemical response of the PEC biosensor. The influence of pH of the phosphate buffer on the cathodic current peak of RTN was evaluated in the range of 4.0–8.0. From the results shown in Fig. 3a, the highest voltammetric response for RTN was registered at pH 6.0, which was used in further biosensing studies. At higher pH values, OH^- binds to the T1-Cu site of laccase, inhibiting the internal transfer of electrons to the T2-Cu and T3-Cu centers [36]. As a result of this phenomenon, the stability of enzyme activity is compromised, and not usable for biosensing applications. In addition, Fig. 3b shows the linear variation between the peak potential and the PB's pH with a slope of − 55.9 mV/pH ($R^2 = 0.999$); a value very close to that expected for a Nernstian system with two electrons and two protons involved as described in other studies reported the literature for RTN [31].

The instrumental parameters for SW voltammetric determination of RTN were optimized in order to obtain a high degree of sensitivity for the biosensing analyses. The parameters included: *f*: 10–80 Hz, *a*: 10–80 Hz, and ΔE_S: 1–6 mV. The optimum values observed ($f = 50$ Hz, $a = 50$ mV, $\Delta E_S = 3$ mV) were used to record the analytical curve of RTN in PB (pH 6.0).

The analytical curve obtained from the resultant cathodic peak current (measured at 0.33 V vs. Ag/AgCl) from the electrochemical reduction of *o*-quinone was recorded in the SW voltammograms shown in Fig. 4a (*light-off*) and Fig. 4b (*light-on*), as a function of the concentration of RTN. A linear relationship was observed between peak

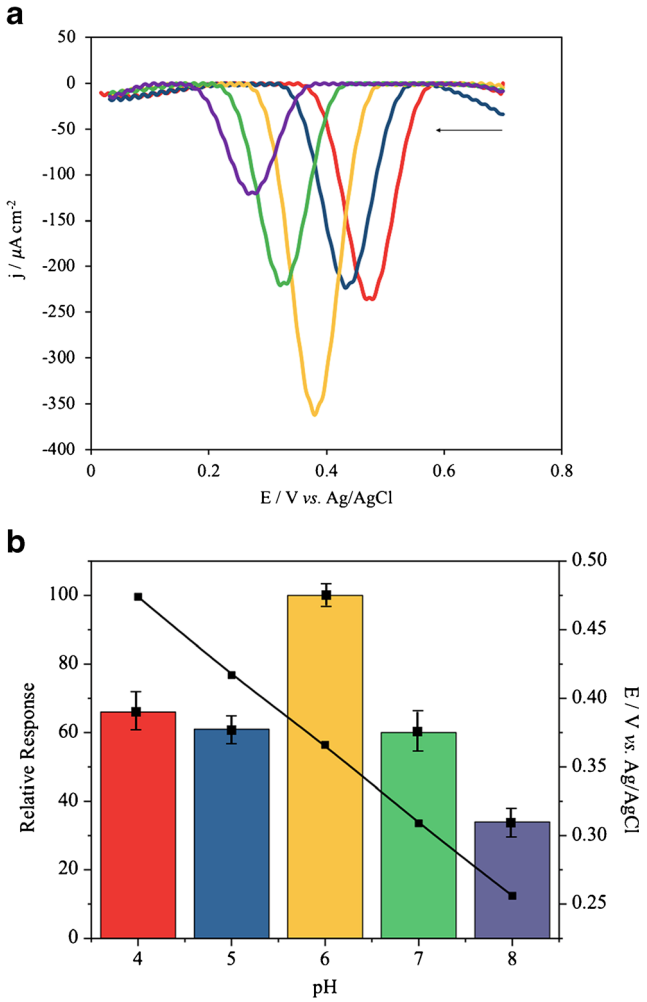

Fig. 3 (**a**) SW voltammograms recorded using the GCE/(α-Fe_2O_3.PdNPs)-LCE biosensor with 99.0 μmol L^{-1} rutin in PB at different pH values: 4.0 to 8.0. (**b**) Influence of the pH on the cathodic peak current (bars) and the peak potential (black line) of the PEC biosensor. The conditions of SWV were the same as those indicated in Fig. 2

current (μA) and the concentration of RTN ranging from 0.052–38.5 × 10^{-8} mol L^{-1} (Fig. 4a, *inset*), and 0.008–30.0 × 10^{-8} mol L^{-1} (Fig. 4b, *inset*). The following respective linear regression equations were recorded: j (μA cm^{-2}) = 1.1 + 0.7 [c (× 10^{-8} mol L^{-1})] (R^2 = 0.999), and j (μA cm^{-2}) = 1.3 + 1.7 [c (× 10^{-8} mol L^{-1})] (R^2 = 0.999); where j is the current density measured at 0.33 V vs. Ag/AgCl, and c the RTN concentration. The LOD values obtained for the *light-off* and *light-on* modes were respectively, 5.2 × 10^{-10} mol L^{-1} and 8.4 × 10^{-11} mol L^{-1}. As observed in Fig. 4b (*inset*), a higher sensitivity resulted in employing the PEC biosensor under visible light

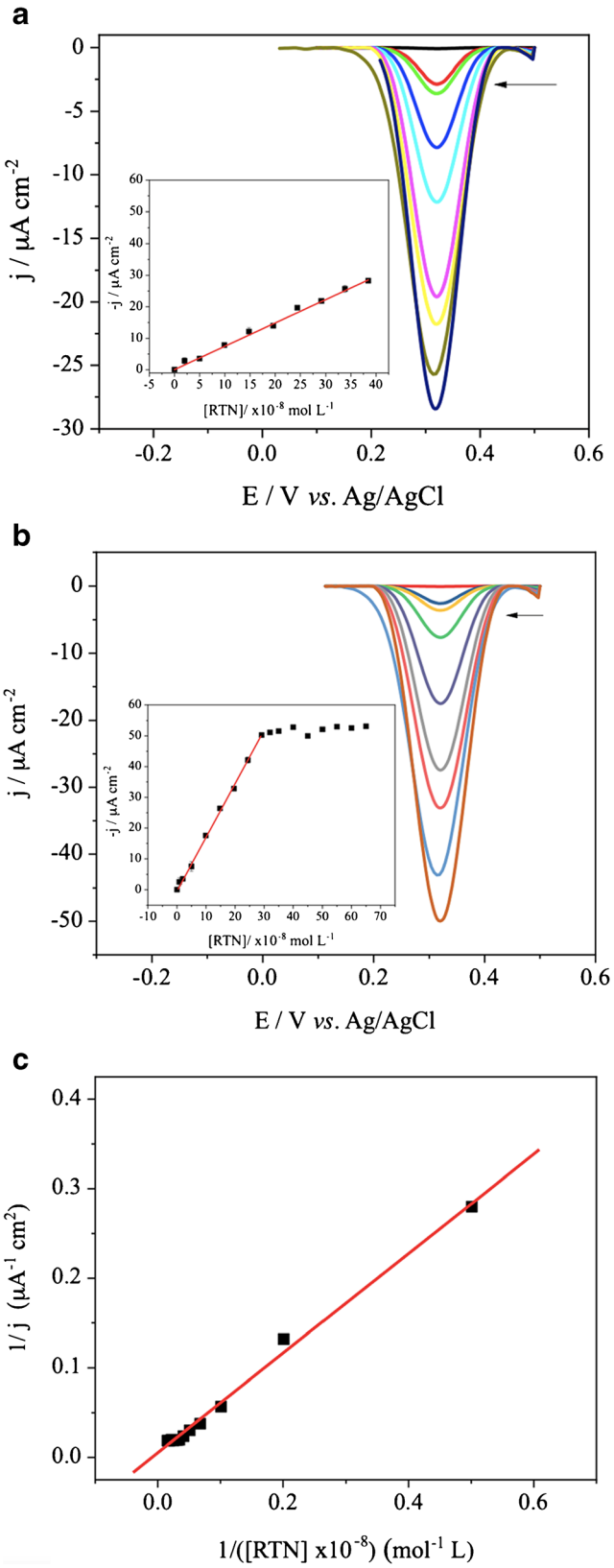

Fig. 4 SW voltammograms obtained in PB (pH 6.0) employing GCE/(α-Fe_2O_3.PdNPs)-LCE as the working electrode: (**a**) *light-off* mode at the following concentrations of rutin: 0.0–38.5 × 10^{-8} mol L^{-1} (E = 0.33 V vs. Ag/AgCl), (**b**) *light-on* mode at the following concentrations of rutin: 0.0–30.0 × 10^{-8} mol L^{-1} (E = 0.33 V vs. Ag/AgCl), and (**c**) Lineweaver-Burk plot. SWV parameters: f = 50 Hz, a = 50 mV, and ΔE_S = 3 mV. *Inset*: (**a** and **b**) corresponding analytical curves

excitation (*light-on* condition). This result is attributable to the efficient photoelectrocatalytic mechanism for signal amplification as discussed above.

For the determination of the kinetic parameter of the enzyme-based PEC biosensor, the apparent Michaelis-Menten constant was calculated by plotting the variation of the current density versus concentration of rutin and using the electrochemical Michaelis-Menten equation:

$$j = \frac{j_{\max}[S]}{K_m^{\text{app}}} \quad (1)$$

where $[S]$ is the substrate concentration ([RTN]), $j_{\max}$ is the maximum current density and K_m^{app} represents the apparent Michaelis-Menten constant. Figure 4b (*inset*) shows the variation of the current density versus rutin concentration (0.0–65.0×10^{-8} mol L^{-1}) and the Lineweaver-Burk graph is shown in Fig. 4c. As can be seen in Fig. 4b (*inset*), the current density response deviated from linearity and reached a constant value at high rutin concentrations. This is attributed to the maximum rate of the enzymatic reaction under rutin saturating conditions. The apparent Michaelis-Menten constant was estimated using the Lineweaver-Burk equation and a value of K_m^{app} = 2.7 nmol L^{-1} was obtained.

The repeatability of the electrochemical measurements was performed using the constructed PEC biosensor and evaluated by monitoring the cathodic current by SWV in PB (pH 6.0) using 1.08×10^{-7} mol L^{-1} RTN. After ten successive measurements using the same device, without any superficial renovation, the current signals showed a 0.21% SD (*light-on* mode). This confirmed the stability of the photoactive biocatalytic surface and demonstrated that the biosensor can be used in repetitive analyses providing precise measurements.

The reproducibility of the biosensing platform assembly was evaluated by monitoring the voltammetric signals (*light-on* mode) of three independently-constructed GCE/(α-Fe_2O_3.PdNPs)-LCE biosensors at 1.08×10^{-7} mol L^{-1} of RTN in PB (pH 6.0). This study provided a SD of 1.3% between the electrochemical measurements of the three devices, indicating excellent reproduction in the PEC biosensor construction.

The analytical parameters of the GCE/(α-Fe_2O_3.PdNPs)-LCE biosensor device was compared with those previously reported for (bio)sensors used to quantify RTN and is shown in Table 1. The comparative analysis suggests that the PEC biosensor presents a remarkable electroanalytical performance regarding the LOD and linear range examined, providing stable and selective measurements from an enzyme-based reaction. Additionally, the device proposed herein presented high simplicity in the immobilization of enzyme, without using any mediators and coupling agents required to link the enzyme onto the photoactive material (α-Fe_2O_3.PdNPs). Therefore, this biosensor, as well as the proposed enzyme immobilization method, was demonstrated to be promising in the development of a selective photoelectrochemical method for the determination of RTN.

Selectivity and analytical application of the GCE/(α-Fe_2O_3.PdNPs)-LCE biosensor for the determination of rutin

The substrate specificity/selectivity was evaluated based on the electrochemical reduction of *o*-quinone to RTN ($1.08 \times$

Table 1 Comparison of results obtained for the determination of rutin using the photoelectrochemical biosensor (*light-on* mode) and (bio)sensors reported in the scientific literature

(Bio)sensor	Linear range (μmol L^{-1})	LOD (μmol L^{-1})	Features of the methods	Reference
GR-MnO_2/CILE	0.01–500	3.0×10^{-3}	- Rapid determination; but is not selective.	[37]
CH(TPP)-LCE	0.6–3.92	6.0×10^{-2}	- Simple method for enzyme immobilization; selectivity.	[30]
BMI.Tf_2N-LCE	4.77–46.2	4.5×10^{-1}	- Time-consuming for electrode preparation; selectivity.	[31]
SH-β-CD-GR/PdNPs	1.0×10^{-3}–30	3.0×10^{-4}	- Time-consuming for electrode preparation; selectivity problems.	[38]
GCE/NH_2-Fe_3O_4 NPs-ErGO	6.0×10^{-3}–80	4.0×10^{-3}	- Tedious electrode preparation; accumulation time of 210 s; selectivity.	[39]
Polyfurfural film/GCE	1.0×10^{-3}–10	2.5×10^{-5}	- Low LOD; selectivity problems.	[40]
GCE/(α-Fe_2O_3.PdNPs)-LCE	8.4×10^{-5}–0.3	8.4×10^{-5}	- Low LOD; efficient method for enzyme immobilization; selectivity.	This work

GR: graphene; *CILE*: carbon ionic liquid electrode; *CH*: chitosan; *TPP*: sodium tripolyphosphate; *BMI*: 1-butyl-3-methylimidazolium; *Tf_2N*: bis(trifluoromethylsulfonyl)imide; *SH-β-CD*: thiol (β)-cyclodextrin; *NH_2-Fe_3O_4 NPs*: amine-functionalized Fe_3O_4 nanoparticles; *ErGO*: electrochemically reduced graphene oxide

Table 2 Rutin content of commercial beverage samples determined using the PEC biosensor and compared with HPLC analysis

Beverage sample	Rutin amount (mg L^{-1}) [a]			
	GCE/(α-Fe_2O_3.PdNPs)-LCE	HPLC	E (%)[b]	F_{calc}[c]
Green tea	14.9 ± 0.2	15.2 ± 0.1	− 2.0	4.0
Red wine	8.0 ± 0.3	7.8 ± 0.3	+ 2.4	1.0

[a] Average of three measurements

[b] 100 × [(LCE biosensor − HPLC method)/HPLC method]

[c] Critical F value = 19.0 (95% confidence level)

10^{-7} mol L^{-1}) by SWV, in the presence of related phenol-model compounds: epinephrine, dopamine, paracetamol, guaiacol, catechol, hydroquinone, phenylamine, quercetin, chlorogenic acid, ferulic acid, gallic acid, coumaric acid, caffeic acid, and quinic acid (concentration ratio of RTN-to-other chemical species at 1:10). As shown in Fig. ESM6, no significant changes were observed in the voltammetric current signals associated with RTN (SD < 1.0%) as the cathodic signals for each phenolic compound analyzed did not overlap with the RTN peak. In addition, the selectivity of the PEC biosensor was evaluated in the presence of different chemical species, including uric acid and some inorganic ions commonly found as complexes (Ca^{2+}, Mn^{2+}, Fe^{2+}, Zn^{2+}, SO_4^{2-}, and NO^{3-}). Even under these conditions, the PEC biosensor presented a stable and reproducible response for the electrochemical reduction of *o*-quinone (RSD < 3%).

In order to verify the applicability of the GCE/(α-Fe_2O_3.PdNPs)-LCE (*light-on* mode) PEC biosensor in real samples, RTN was determined in commercial green tea and red wine; common flavonoid-containing beverages. Fig. ESM7 presents the SW voltammograms obtained by the standard addition method for (a) green tea and (b) red wine. A linear signal response for both samples was achieved in the concentration range of 0.0 to 24.2 × 10^{-8} mol L^{-1}, based on the equations: (a) j (μA cm^{-2}) = 55.7 + 1.1 [c (× 10^{-8} mol L^{-1})] (R^2 = 0.998), and (b) j (μA cm^{-2}) = 50.7 + 1.6 [c (× 10^{-8} mol L^{-1})] (R^2 = 0.998).

The analyses of green tea and red wine were performed in triplicate, and the results are summarized in Table 2. As can be seen, no significant differences were observed between the RTN concentration found employing the proposed PEC biosensor and the HPLC method [33]. Based upon the F test [41], the proposed biosensor achieved an equivalent level of precision of the HPLC analysis, at the 95% confidence level. All calculated values were lower than the standard value ($F_{critical}$ = 19.0). Applying the paired t test [42] to the data obtained employing both methods, the calculated t value (t = 1.13) was smaller than the critical value (2.57, α = 0.05). Therefore, according to these studies, either method is statistically equivalent, at the 95% confidence level.

The PEC biosensor (*light-on* mode) was also employed to detect and determine RTN in a biological fluid (human urine). The samples were spiked with two different concentrations of RTN: 1.0 and 3.0 mg L^{-1}. Excellent recovery values close to 100% were achieved (96.5% and 102.3%, respectively). Although the proposed PEC biosensor is based on a weak adsorption method for enzyme immobilization, these results in addition to the food analysis, ensured that the proposed PEC bioelectronic device presents a high degree of accuracy for the quantitative and selective analysis of this polyphenol with satisfactory reversibility and storage lifetime.

Conclusion

The proposed photoelectrochemical device (GCE/(α-Fe_2O_3.PdNPs)-LCE) was successfully fabricated. The photoactive support was prepared based upon the precipitation of ferrite microcubes employing $Zn(CH_3CO_2)_2$ as the structure-directing agent. The functionalized hematite (α-Fe_2O_3.PdNPs) exhibited largely enhanced photoelectrocatalytic signals towards the electroactive species, along with the high biocompatibility for the immobilization of the enzyme laccase, providing satisfactory reproducibility and long-term stability. The quantitative analyses of RTN in complex samples (beverages and biological fluids) did not require any physical/chemical pretreatment. The addition and recovery studies on human urine confirmed that the proposed biosensor is highly selective, since no interference from other biochemical compounds in these samples was observed. According to statistical studies, the results for the biosensing analysis of commercial beverages containing RTN were in agreement with HPLC determinations at the 95% confidence level. Moreover, the bioelectronic device based on the efficient integration of a photoactive material and a biocatalyst appears to have wide applications in selective electroanalysis, providing fast response times, and high sensitivity.

Supplementary Information The online version contains supplementary material available at https://doi.org/10.1007/s00604-020-04659-z.

Acknowledgments The authors gratefully acknowledge the financial support and scholarships from the Brazilian funding agencies CNPq

(grant nos. 408591/2018-8; 305320/2019-0; Dr. E. R. Sartori), Fundação Araucária do Paraná, and CAPES (grant no. 88882.448537/2019/01; C. A. R. Salamanca-Neto). Dr. A. M. Barbosa-Dekker is grateful to CNPq (Proc. 309717/2015-9) and Fundação Araucária for a senior scholarship. E. C. M. Barbosa thanks FAPESP for a doctorate scholarship (grant no. 2015/11452-5). Dr. P. H. C. Camargo thanks FAPESP for grants (no. 2015/21366-9 and 2015/26308-7).

Compliance with ethical standards

Conflict of interest The authors declare that they have no competing interests.

References

1. Devadoss A, Sudhagar P, Terashima C, Nakata K, Fujishima A (2015) Photoelectrochemical biosensors: new insights into promising photoelectrodes and signal amplification strategies. J Photochem Photobiol C: Photochem Rev 24:43–63. https://doi.org/10.1016/j.jphotochemrev.2015.06.002
2. Zhang C, Si S, Yang Z (2015) A highly selective photoelectrochemical biosensor for uric acid based on core–shell Fe3O4@C nanoparticle and molecularly imprinted TiO2. Biosens Bioelectron 65:115–120. https://doi.org/10.1016/J.BIOS.2014.10.013
3. Dilgin DG, Ismet Gökçel H (2015) Photoelectrochemical glucose biosensor in flow injection analysis system based on glucose dehydrogenase immobilized on poly-hematoxylin modified glassy carbon electrode. Anal Methods 7:990–999. https://doi.org/10.1039/c4ay02269f
4. Zhang L, Mohamed HH, Dillert R, Bahnemann D (2012) Kinetics and mechanisms of charge transfer processes in photocatalytic systems: a review. J Photochem Photobiol C: Photochem Rev 13:263–276. https://doi.org/10.1016/J.JPHOTOCHEMREV.2012.07.002
5. Zhang X, Zhang R, Yang A, Wang Q, Kong R, Qu F (2017) Aptamer based photoelectrochemical determination of tetracycline using a spindle-like ZnO-CdS@Au nanocomposite. Microchim Acta 184:4367–4374. https://doi.org/10.1007/s00604-017-2477-8
6. Atchudan R, Muthuchamy N, Edison TNJI, Perumal S, Vinodh R, Park KH, Lee YR (2019) An ultrasensitive photoelectrochemical biosensor for glucose based on bio-derived nitrogen-doped carbon sheets wrapped titanium dioxide nanoparticles. Biosens Bioelectron 126:160–169. https://doi.org/10.1016/J.BIOS.2018.10.049
7. Muthuchamy N, Lee K-P, Gopalan A-I (2017) Enhanced photoelectrochemical biosensing performances for graphene (2D) – titanium dioxide nanowire (1D) heterojunction polymer conductive nanosponges. Biosens Bioelectron 89:390–399. https://doi.org/10.1016/J.BIOS.2016.06.005
8. Tu W, Dong Y, Lei J, Ju H (2010) Low-potential Photoelectrochemical biosensing using porphyrin-functionalized TiO 2 nanoparticles. Anal Chem 82:8711–8716
9. Roy S (2017) Impact of UV radiation on genome stability and human health. Adv Exp Med Biol 996:207–219. https://doi.org/10.1007/978-3-319-56017-5_17
10. Mirzaei A, Hashemi B, Janghorban K (2016) α-Fe2O3 based nanomaterials as gas sensors. J Mater Sci Mater Electron 27:3109–3144. https://doi.org/10.1007/s10854-015-4200-z
11. Cuong ND, Khieu DQ, Hoa TT, Quang DT, Viet PH, Lam TD, Hoa ND, Hieu NV (2015) Facile synthesis of α-Fe2O3 nanoparticles for high-performance CO gas sensor. Mater Res Bull 68:302–307. https://doi.org/10.1016/J.MATERRESBULL.2015.03.069
12. Khorram R, Raissi H, Morsali A, Shahabi M (2019) The computational study of the γ-Fe 2 O 3 nanoparticle as Carmustine drug delivery system: DFT approach. J Biomol Struct Dyn 37:454–464. https://doi.org/10.1080/07391102.2018.1429312
13. Pailhé N, Wattiaux A, Gaudon M, Demourgues A (2008) Impact of structural features on pigment properties of α-Fe2O3 haematite. J Solid State Chem 181:2697–2704. https://doi.org/10.1016/J.JSSC.2008.06.049
14. Wang L, Lee C-Y, Schmuki P (2013) Influence of annealing temperature on photoelectrochemical water splitting of α-Fe2O3 films prepared by anodic deposition. Electrochim Acta 91:307–313. https://doi.org/10.1016/J.ELECTACTA.2012.12.101
15. Song X-M, Zhou X, Yuan C, Zhang Y, Tong Q, Li Y, Cui L, Liu D, Zhang W (2017) One-dimensional Fe2O3/TiO2 photoelectrode and investigation of its photoelectric properties in photoelectrochemical cell. Appl Surf Sci 397:112–118. https://doi.org/10.1016/J.APSUSC.2016.11.143
16. Patel SKS, Anwar MZ, Kumar A, Otari SV, Pagolu RT, Kim SY, Kim IW, Lee JK (2018) Fe2O3 yolk-shell particle-based laccase biosensor for efficient detection of 2,6-dimethoxyphenol. Biochem Eng J 132:1–8. https://doi.org/10.1016/J.BEJ.2017.12.013
17. Umar A, Ahmad R, Hwang SW, Kim SH, al-Hajry A, Hahn YB (2014) Development of highly sensitive and selective cholesterol biosensor based on cholesterol oxidase co-immobilized with α-Fe2O3 micro-pine shaped hierarchical structures. Electrochim Acta 135:396–403. https://doi.org/10.1016/J.ELECTACTA.2014.04.173
18. Zhang J, Liu X, Guo X et al (2010) A general approach to fabricate diverse noble-metal (Au, Pt, Ag, Pt/Au)/Fe 2 O 3 hybrid nanomaterials. Chem Euro J 16:8108–8116. https://doi.org/10.1002/chem.201000096
19. Momeni MM, Hallaj A, Ghayeb Y, Bagheri R, Song Z, Farrokhpour H (2019) Extended light absorption and enhanced photoelectrochemical activity of palladium-decorated hematite nanotubes prepared by photodeposition method. Appl Organomet Chem 33:1–8. https://doi.org/10.1002/aoc.5087
20. Zhao WW, Xu JJ, Chen HY (2015) Photoelectrochemical bioanalysis: the state of the art. Chem Soc Rev 44:729–741. https://doi.org/10.1039/c4cs00228h
21. Cannatelli MD, Ragauskas AJ (2017) Two decades of laccases: advancing sustainability in the chemical industry. Chem Rec 17:122–140. https://doi.org/10.1002/tcr.201600033
22. Mattos GJ, Moraes JT, Barbosa ECM, Camargo PHC, Dekker RFH, Barbosa-Dekker AM, Sartori ER (2019) Laccase stabilized on β-D-glucan films on the surface of carbon black/gold nanoparticles: a new platform for electrochemical biosensing. Bioelectrochemistry. 129:116–123. https://doi.org/10.1016/J.BIOELECHEM.2019.05.002
23. Coelho JH, Eisele APP, Valezi CF, Mattos GJ, Schirmann JG, Dekker RFH, Barbosa-Dekker AM, Sartori ER (2019) Exploring the exocellular fungal biopolymer botryosphaeran for laccase-biosensor architecture and application to determine dopamine and spironolactone. Talanta. 204:475–483. https://doi.org/10.1016/j.talanta.2019.06.033
24. Vasconcelos AFD, Barbosa AM, Dekker RFH, Scarminio IS, Rezende MI (2000) Optimization of laccase production by *Botryosphaeria* sp. in the presence of veratryl alcohol by the response-surface method. Process Biochem 35:1131–1138. https://doi.org/10.1016/S0032-9592(00)00149-7
25. Wong SP, Leong LP, William Koh JH (2006) Antioxidant activities of aqueous extracts of selected plants. Food Chem 99:775–783. https://doi.org/10.1016/J.FOODCHEM.2005.07.058
26. Yang N, Ren G (2008) Application of near-infrared reflectance spectroscopy to the evaluation of rutin and D-chiro-inositol contents in tartary buckwheat. J Agric Food Chem 56:761–764. https://doi.org/10.1021/jf072453u
27. Mao Z, Shan R, Wang J, Cai W, Shao X (2014) Optimizing the models for rapid determination of chlorogenic acid, scopoletin and

rutin in plant samples by near-infrared diffuse reflectance spectroscopy. Spectrochim Acta Part A Mol Biomol Spectrosc 128:711–715. https://doi.org/10.1016/J.SAA.2014.03.015
28. Ishii K, Furuta T, Kasuya Y (2001) Determination of rutin in human plasma by high-performance liquid chromatography utilizing solid-phase extraction and ultraviolet detection. J Chromatogr B Biomed Sci Appl 759:161–168. https://doi.org/10.1016/S0378-4347(01)00224-9
29. Zu Y, Li C, Fu Y, Zhao C (2006) Simultaneous determination of catechin, rutin, quercetin kaempferol and isorhamnetin in the extract of sea buckthorn (Hippophae rhamnoides L.) leaves by RP-HPLC with DAD. J Pharm Biomed Anal 41:714–719. https://doi.org/10.1016/J.JPBA.2005.04.052
30. Fernandes SC, de Oliveira IRWZ, Fatibello-Filho O, Spinelli A, Vieira IC (2008) Biosensor based on laccase immobilized on microspheres of chitosan crosslinked with tripolyphosphate. Sensors Actuators B Chem 133:202–207. https://doi.org/10.1016/j.snb.2008.02.023
31. Franzoi AC, Migowski P, Dupont J, Vieira IC (2009) Development of biosensors containing laccase and imidazolium bis(trifluoromethylsulfonyl)imide ionic liquid for the determination of rutin. Anal Chim Acta 639:90–95. https://doi.org/10.1016/j.aca.2009.03.012
32. Dekker RFH, Barbosa AM (2001) The effects of aeration and veratryl alcohol on the production of two laccases by the ascomycete *Botryosphaeria* sp. Enzym Microb Technol 28:81–88
33. Tarola AM, Milano F, Giannetti V (2007) Simultaneous determination of phenolic compounds in red wines by HPLC-UV. Anal Lett 40:2433–2445. https://doi.org/10.1080/00032710701577666
34. Viswanath B, Rajesh B, Janardhan A, Kumar AP, Narasimha G (2014) Fungal laccases and their applications in bioremediation. Enzyme Res 2014:163242–163221. https://doi.org/10.1155/2014/163242
35. El Hatimi A, Gómez M, Jansat S et al (1998) Chiral bis(oxazoline) ligands. Synthesis of mono- and bi-metallic complexes of nickel and palladium. J Chem Soc Dalton Trans 1998:4229–4236. https://doi.org/10.1039/a807946c
36. Xu F (1997) Effects of redox potential and hydroxide inhibition on the pH activity profile of fungal laccases. J Biol Chem 272:924–928. https://doi.org/10.1074/JBC.272.2.924
37. Sun W, Wang X, Zhu H, Sun X, Shi F, Li G, Sun Z (2013) Graphene-MnO2 nanocomposite modified carbon ionic liquid electrode for the sensitive electrochemical detection of rutin. Sensors Actuators B Chem 178:443–449. https://doi.org/10.1016/J.SNB.2012.12.118
38. Liu Z, Xue Q, Guo Y (2017) Sensitive electrochemical detection of rutin and isoquercitrin based on SH-β-cyclodextrin functionalized graphene-palladium nanoparticles. Biosens Bioelectron 89:444–452. https://doi.org/10.1016/J.BIOS.2016.04.056
39. He Q, Wu Y, Tian Y, Li G, Liu J, Deng P, Chen D (2019) Facile electrochemical sensor for nanomolar rutin detection based on magnetite nanoparticles and reduced graphene oxide decorated electrode. Nanomaterials 9:115. https://doi.org/10.3390/nano9010115
40. Huang J, Shen X, Hu Q, Ma Y, Bai S, Yue G, Yu X, Zeng Q, Wang L (2016) High sensitivity simultaneous determination of myricetin and rutin using a polyfurfural film modified glassy carbon electrode. RSC Adv 6:95435–95441. https://doi.org/10.1039/c6ra20459g
41. Ellison SLR, Barwick VJ, Farrant TJD (2009) Practical statistics for the analytical scientist. Royal Society of Chemistry, Cambridge
42. Anderson RL (1987) Practical statistics for analytical chemists. Van Nostrand Reinhold, New York